International Journal of Computational Bioinformatics and In Silico Modeling
Vol. 3, No. 6 (2014): 525-530
Research Article
Open Access

ISSN: 2320-0634

Structural insight into the homology modeled human N-acetyl-alpha-neuraminidase 3 (NEU3)

Hideaki Yamaguchi*

Department of Pharmacy, Faculty of Pharmacy, Meijo University, 150 Yagotoyama, Tenpaku, Nagoya 468-8503, Japan

*Corresponding author: Hideaki Yamaguchi; e-mail: hyamagu@meijo-u.ac.jp

Received: 01 September 2014 Accepted: 28 October 2014 Online: 01 November 2014

ABSTRACT

This is a sequel to the previous study in homology modeling and structural analysis of human N-acetyl-alpha-neuraminidase 3 (NEU3). Further analysis was performed with a software package the Molecular Operating Environment. A human NEU2 (PDB code: 1VCU) was selected as a template for the 3D structure modeling of NEU3. The superimposition and root mean square deviation analysis indicated that the modeled NEU3 showed significant 2D and 3D similarities to NEU2. The molecular electrostatic potential (MEP) map of the NEU3 model exhibited that the model was different from the NEU2 model electrostatically at the LBS. Further, docking simulations revealed the similarity of the ligand-receptor bound location between the NEU2 and 3 models. The different binding orientations between the N-acetyl-2,3-dehydro-2-deoxyneuraminic acid (DANA)-NEU2 and DANA-NEU3 complexes reflected the different MEP maps at the LBSs between the NEU2 and 3 models. The docking simulation revealed that DANA possibly inhibits functions of NEU3 interfering with Arg25 and Asn88. These results indicate that the NEU3 model was successfully modeled and analyzed. Our data verify that the model can be utilized for application to target NEU3 for the development of anticancer drugs.

Keywords: N-acetyl-alpha-neuraminidase 3 (NEU3), cancer, *in silico*.

INTRODUCTION

Gangliosides are commonly found in the outer leaflet of the plasma membrane bilayer and contain sialic acids with their sugar chains extend out from the cell surface [1]. Gangliosides have been considered to play important roles in different biological events, such as cell-to-cell interactions and signal transduction [2,3]. They have also been reported to induce immune cell dysfunction [4]. Crucial roles played by gangliosides were recognized in the development of cancer. In particular, monosialosyl galactosylgloboside increased metastatic potential and was inversely correlated with patient survival with renal cell carcinoma [5]. GD3 ganglioside and its derivatives have also been demonstrated to promote melanoma cell proliferation and invasion [6-9]. Moreover, GM3 ganglioside and its variants have been suggested to interact with microtubules and intermediate filaments and also bind to epidermal growth factor receptor (EGFR), regulating cancer cell migration, invasion and the activity of EGFR [1-3,10,11]. The poor expression of gangliosides in normal cells and their higher expression in cancer cells also suggest that they play important roles in development and progression of cancer [7,12].

The alteration of the enzymatic mechanisms that regulate ganglioside synthesis could be critical in determining the cancer cell ganglioside composition. In particular, α-2,3-sialyltransferase, α-2,8-sialyl transferase and β-1,4-N-acetylegalactosaminyl transferase have been reported to be deregulated in cancer cells [5,8,13,14]. Similarly, the plasma membrane-associated sialidase N-acetyl-alpha-neuraminidase 3 (NEU3, EC = 3.2.1.18) has been shown to be highly altered in cancer cell lines compared with normal cells [15,16]. NEU3 was ascribed to the enzyme responsible for the modifications of the ganglioside composition in the membrane and considered as a modulator of AKT phosphorylation [17]. Aberrant overexpression of NEU3 was observed in several neoplastic conditions, such as colon, ovarian, renal, prostate and skin cancer, and NEU3 was attributed to

be one of the key triggers of cancer development and progression [9,15,16,18].

In the previous report, homology modeling and structural analysis of NEU3 were performed with a software package the Molecular Operating Environment (MOE), utilizing a human NEU2 (PDB code: 1SNT) as a template for the 3D structure modeling of NEU3 [19]. The modeled NEU3 showed significant 2D and 3D similarities to NEU2, and the contact energy profiles of the NEU3 model were in good agreement with those of the NEU2 structure. Furthermore, Ramachandran plots revealed that only 2.5% of the amino acid residues were in the disfavored region for NEU3 [19]. In the present study, further structural analysis of the homology modeled NEU3, focusing on the structural comparisons of the NEU models, electrostatic potential surfaces and ligand-protein interactions, will be presented.

MATERIALS AND METHODS

Homology modeling of NEU3

Homology modeling of NEU3 was executed as previously reported [19]. In brief, the NEU3 (NCBI reference sequence: NM_006656) [20] and the crystal structure coordinates of NEU2 (PDB code: 1VCU) [21] were loaded into the MOE. The primary structures of NEU2 and NEU3 were aligned, carefully checked to avoid deletions or insertions in conserved regions and corrected wherever necessary. A series of the NEU3 model were independently constructed with the MOE using a Boltzmann-weighted randomized procedure [22] combined with specialized logic for the handling of sequence insertions and deletions [23]. There were no differences in the numbers and organizations of the secondary structural elements and no significant main chain deviations among the 10 models generated for NEU3. The model with the best packing quality function was selected in the study for full energy minimization and further inspection.

Assessment of the modeled structure

Assessment of the modeled structure of NEU3 was executed as previously reported [19]. In brief, the overall geometric and stereochemical qualities of the final modeled structure of NEU3 were examined using Ramachandran plots generated within the MOE [24,25]. The qualities of the protein folds of the NEU3 homology model were evaluated with the MOE by calculating the effective atomic contact energies, comprising the desolvation free energies required to transfer atoms from water to the interior of the protein [26]. Briefly, the contact desolvation energies were calculated for 18 different atom types of the 20 common amino acids that were resolved based on the clustering pattern of their properties. The contact potentials for each atom type were measured within a contact range of 6 Å by explicitly accounting for neighboring interactions.

Molecular electrostatic potential (MEP) mapping

Electrostatic potential surfaces were calculated by solving the nonlinear Poisson-Boltzmann equation using a finite difference method as implemented in the MOE. The molecular electrostatic interactions form a crucial part of the non-covalent interaction energy between the molecules. The MEP on a molecular surface can be used to visually compare different molecules, analyze docking studies and identify sites that interact with ligands. For example, the surface MEP was utilized to relate a nucleotide mutation with the potential values [27]. In the present study, the MEP was colored in deep blue to indicate the most positive potential and in deep red to represent the most negative potential.

Binding site selection and exploration

The binding site selection and exploration for NEU3 was executed as previously reported [28]. In brief, the Site Finder module of the MOE was used to identify possible substrate-binding pockets within the newly generated 3D structures of NEU3. Hydrophobic or hydrophilic alpha spheres served as probes denoting zones of tight atom packing. These alpha spheres were utilized to define potential ligand-binding sites (LBSs) and as centroids for the creation of dummy ligand atoms [29,30]. The dummy atoms were matched to the corresponding alpha spheres during the characterization of the LBSs in NEU3. This method generates bound conformations that approach crystallographic resolutions [31].

Alpha sphere and excluded volume-based ligand-protein docking (ASE-Dock)

The docking and analysis of the ligand-protein interaction between sialic acid and NEU3 were also performed with ASE-Dock in the MOE as previously reported [28]. In brief, in the ASE-Dock module, ligand atoms have alpha spheres within 1 Å. Based on this property, concave models are created and ligand atoms from a large number of conformations generated by superimposition with these points can be evaluated and scored by maximum overlap with alpha spheres and minimum overlap with the receptor atoms. The scoring function used by ASE-Dock is based on ligand-protein interaction energies and the score is expressed as a U_{total} value. The ligand conformations were subjected to energy minimization using the MMFF94S force field [32]. From the resulting 500,000 poses, the 200 poses with the lowest U_{total} values were selected for further optimization with the MMFF94S force field. During the refinement step, the ligand was free to move within the binding pocket.

RESULTS AND DISCUSSION

Structural comparisons of the NEU models

The 1D sequence of NEU2 and 3 were realigned and reinspected for the superimposition analysis in the MOE (Fig. 1). Root mean square deviation (RMSD) values between the main chain atoms of the NEU2 (PDB code: 1VCU) *vs* NEU3 after main chain fit were 1.934 Å. RMSD values for each residue were also analyzed. The RMSD values for the residues located in the LBS were about 2 Å or less (Fig. 2). A superimposition of the template NEU2 (green) and NEU3 (magenta) models

revealed that the NEU models exhibited significant 3D similarities (Fig. 3A). They also presented similar structures at their LBSs (Fig. 3B).

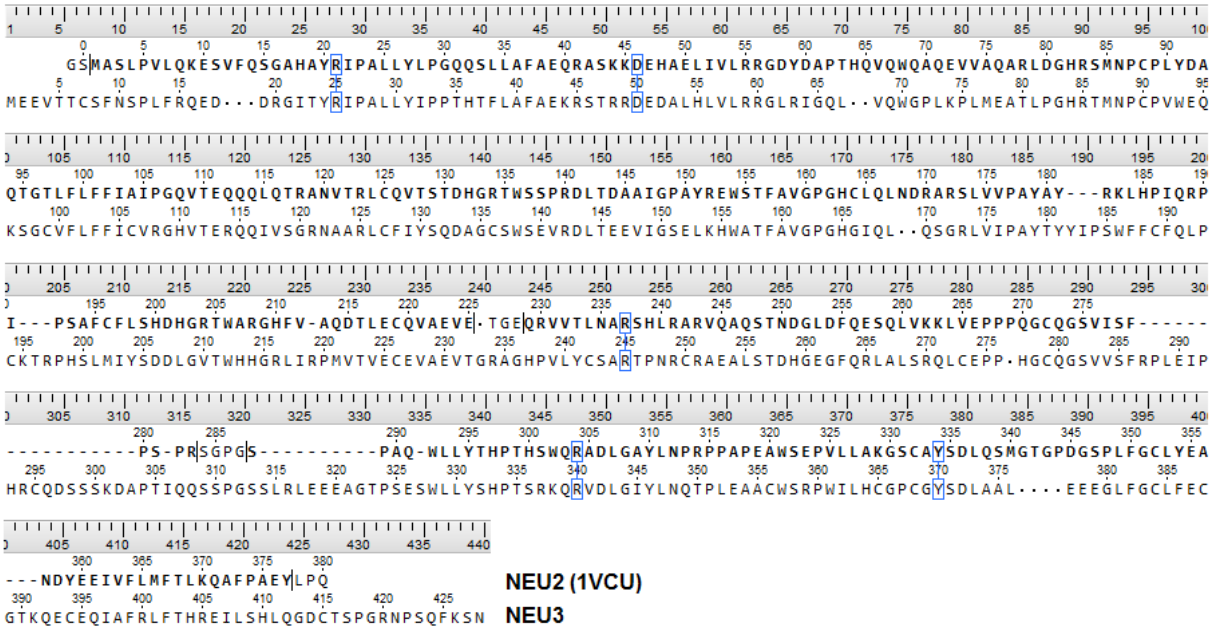

Figure 1. Realigned NEU2 and 3 sequences for the superimposition analysis. The important residues in the LBS are enclosed in blue rectangles. *Upper sequence*: NEU2 (PDB code: 1VCU); *lower sequence*: NEU3.

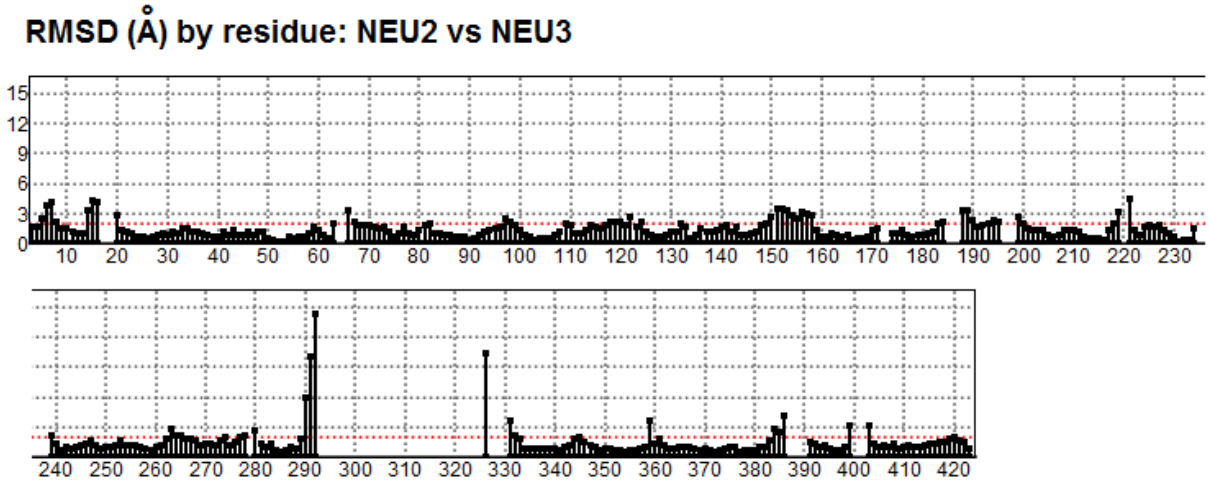

Figure 2. RMSD values between the main chain atoms of the NEU2 *vs* NEU3 after main chain fit. The positions of the amino acid residues are shown on the x-axis, while the RMSD values are shown on the y-axis.

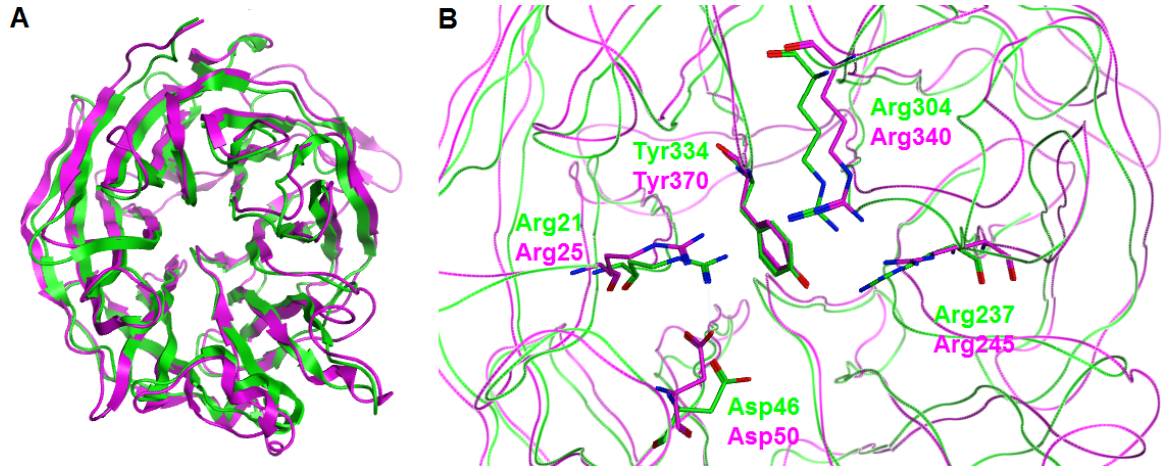

Figure 3. Structural comparison of the NEU models. (A) A superimposition of the template NEU2 (green) and NEU3 (magenta) models. (B) A superimposition of the NEU2 (green) and NEU3 (magenta) models at the LBSs. The important residues in the LBSs are indicated in green for NEU2 and magenta for NEU3.

The MEP maps for the NEU models at LBS

The MEP maps can play a vital role on analyses and predictions of molecular interactive behaviors and properties. For instance, they can be used to compare two molecules visually, which helps in identifying sites that act attractively on ligands by matching opposite electrostatics. Electrostatic interactions are one of the main parts of the interaction energy between ligands and receptors, and govern the strength of non-bonded interactions and molecular reactivity. In the case of a ligand-receptor interaction at the catalytic site, the ligand experiences a unique environment in terms of the electrostatic, steric and hydrophobic properties. Variations in these properties near the catalytic site of receptors can contribute to their selectivity/specificity [33]. The MEP maps of the NEU models are shown in Figure 4. The NEU2 model at the LBS (orange circle) consisted mostly of positive (blue) and slightly hydrophobic (green) spots (Fig. 4A), which indicates that NEU2 possibly attracts hydrophobic and negatively charged parts of ligands at the LBS. On the other hand, the NEU3 model had negative (red) and positive spots at the LBS (Fig. 4B). The differences in the MEP maps between NEU2 and 3 were probably due to the structural differences at and adjacent to the LBSs. These results suggest that binding orientations of ligands at the LBS can be different between NEU2 and 3.

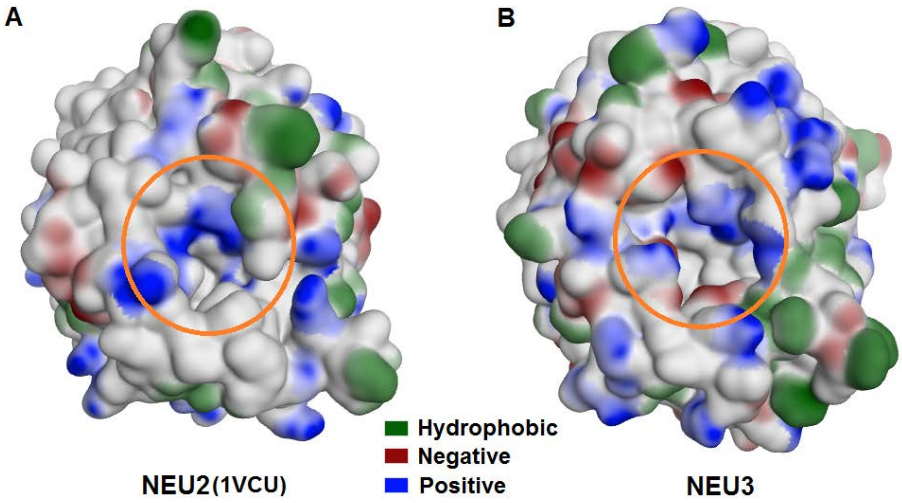

Figure 4. The MEP maps for the NEU models. (A) The MEP map for the NEU2 model. (B) The MEP map for the NEU3 model. The LBSs are enclosed in an orange circle. *Dark green*: hydrophobic spots; *blue*: positive potential spots; *red*: negative potential spots.

Docking simulations of sialic acid to the NEU models

The crystal structure of NEU2 with its substrate N-acetyl-2,3-dehydro-2-deoxyneuraminic acid (DANA) was reported and the substrate recognition of NEU2 was analyzed [21]. However, the precise mode of substrate binding to NEU3 is unknown. The ASE-Dock was performed to evaluate the present docking simulation and showed that DANA bound at the LBS but had a different binding orientation between the NEU2 (Fig. 5A) and NEU3 (Fig. 5B) models. The similarity of the bound location at the LBS between the docked DANA-NEU2 pose and the NEU3 model suggests that the present methods are capable of generating the DANA-NEU3 model similar to the reported near-native NEU2 complex. The results of the different binding orientations of DANA between DANA-NEU2 and DANA-NEU3 complexes reflected the different MEP maps at the LBSs in the NEU models (Fig. 4A and B). This also suggests that the homology modeling of NEU3 and the docking simulations in the present study were performed reasonably well.

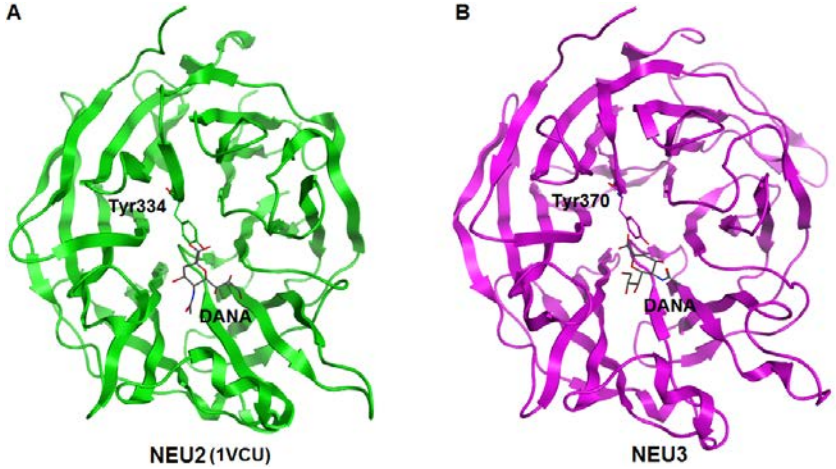

Figure 5. Docking simulations of DANA to the NEU models. (A) ASE-Dock of DANA for NEU2. (B) ASE-Dock of DANA for NEU3. *Blue*: nitrogen; *gray*: carbon; *red*: oxygen.

To create ligand-receptor interaction plots for the DANA-NEU2 and DANA-NEU3 complexes, the Ligand Interactions module of the MOE was used, which provided a clearer arrangement of the key intermolecular interactions that aid in the interpretation of the 3D juxtaposition of DANA and the LBSs in NEU2 and 3. In total, 15 residues were identified as the preferred interaction residues for the DANA and NEU2 complex (Figure 6A). The presence of a hydrogen bond was found between the O1 of DANA and Arg21 and Arg304. The O4 and the O10 of DANA formed the hydrogen bond with Arg237. The NH5 and the C11 of DANA were also identified as the element that formed the hydrogen bond with Glu111. For the DANA and NEU3 complex, 14 residues were identified as the preferred interaction residues (Figure 6B). The presence of a hydrogen bond was found between the O1 of DANA and Arg25. The OH9 of DANA was also identified as the element that formed the hydrogen bond with Asn88.

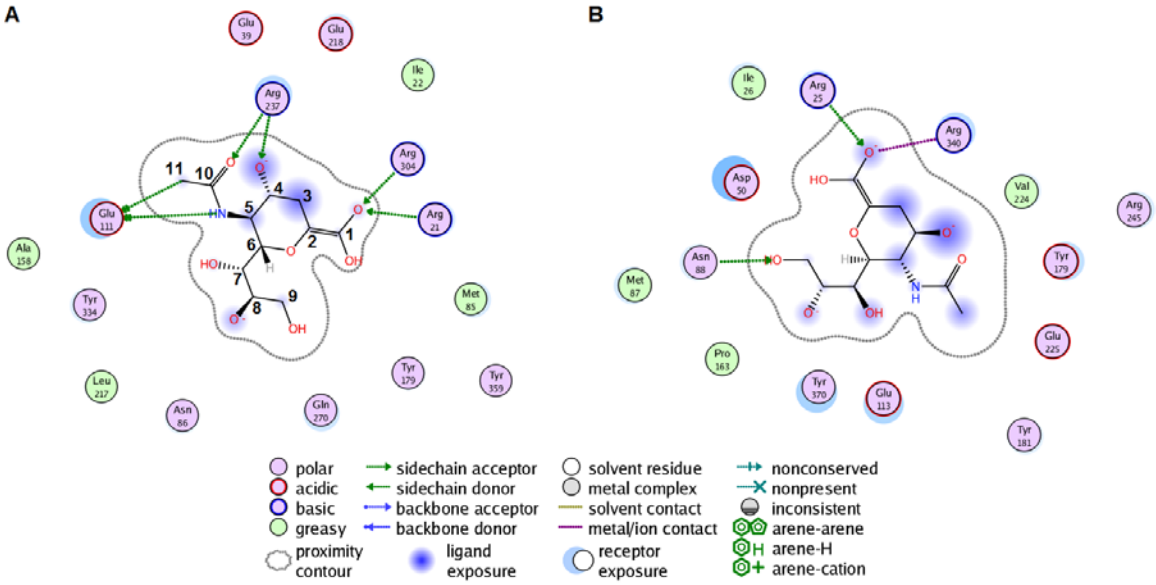

Figure 6. The ligand-receptor interaction plots for the (A) DANA-NEU2 and (B) DANA-NEU3 complexes created by the Ligand Interactions module of the MOE.

CONCLUSION

In the present report, the 3D model of NEU3 was designed using the X-ray crystal structure of NEU2 (PDB code: 1VCU) as a template. The model was successfully evaluated and analyzed in terms of their folding and stereochemical properties. The structural analysis of the NEU3 model was performed and it is proposed that the developed NEU3 model will be suitable for further *in silico* structure-based *de novo* drug designing. The present data verify that the model can be utilized for application to target NEU3 for the development of anticancer drugs.

Acknowledgments

This study was partly supported by a Grant-in-Aid from the Promotion and Mutual Aid Corporation for Private Schools of Japan. My previous report [19] turned out to be NOT THE FIRST REPORT of an NEU3 model. I would like to express my sincere gratitude to Dr. Cairo (University of Alberta) for notifying me of that fact. His recent review should also be referred (Cairo, CW (2014). Inhibitors of the human neuraminidase enzymes. MedChemComm. 5: 1067-1074).

ABBREVIATIONS

ASE-Dock, alpha sphere and excluded volume-based ligand-protein docking; DANA, N-acetyl-2,3-dehydro-2-deoxyneuraminic acid; EGFR, epidermal growth factor receptor; LBS, ligand-binding site; MEP, molecular electrostatic potential; MOE, Molecular Operating Environment; NEU, N-acetyl-alpha-neuraminidase; RMSD, root mean square deviation.

REFERENCES

1. Gillard BK, Thurmon LT and Marcus DM (1993). Variable subcellular localization of glycosphingolipids. Glycobiology. 3: 57-67
2. Wang XQ, Sun P, O'Gorman M, et al (2001). Epidermal growth factor receptor glycosylation is required for ganglioside GM3 binding and GM3-mediated suppression [correction of suppresion] of activation. Glycobiology. 11: 515-522
3. Kawashima N, Yoon S-J, Itoh K, et al (2009). Tyrosine kinase activity of epidermal growth factor receptor is regulated by GM3 binding through carbohydrate to carbohydrate interactions. J Biol Chem. 284: 6147-6155
4. Biswas S, Biswas K, Richmond A, et al (2009). Elevated levels of select gangliosides in T cells from renal cell carcinoma patients is associated with T cell dysfunction. J Immunol. 183: 5050-5058
5. Senda M, Ito A, Tsuchida A, et al (2007). Identification and expression of a sialyltransferase responsible for the synthesis of disialylgalactosylgloboside in normal and malignant kidney cells: downregulation of ST6GalNAc VI in renal cancers. Biochem J. 402: 459-470
6. Portoukalian J, Zwingelstein G and Dore JF (1979). Lipid composition of human malignant melanoma tumors at various levels of malignant growth. Eur J Biochem. 94: 19-23
7. Carubia JM, Yu RK, Macala LJ, et al (1984). Gangliosides of normal and neoplastic human melanocytes. Biochem Biophys Res Commun. 120: 500-504
8. Ruan S, Raj BK and Lloyd KO (1999). Relationship of glycosyltransferases and mRNA levels to ganglioside expression in neuroblastoma and melanoma cells. J Neurochem. 72: 514-521

9. Furukawa K, Hamamura K, Nakashima H, et al (2008). Molecules in the signaling pathway activated by gangliosides can be targets of therapeutics for malignant melanomas. Proteomics. 8: 3312-3316
10. Liu JW, Sun P, Yan Q, et al (2009). De-N-acetyl GM3 promotes melanoma cell migration and invasion through urokinase plasminogen activator receptor signaling-dependent MMP-2 activation. Cancer Res. 69: 8662-8669
11. Blanco R, Rengifo E, Rengifo CE, et al (2011). Cedeno M, Frometa M, Carr A: Immunohistochemical reactivity of the 14F7 monoclonal antibody raised against N-glycolyl GM3 ganglioside in some benign and malignant skin neoplasms. ISRN Dermatol. 2011: 848909
12. Hakomori S (2001). Tumor-associated carbohydrate antigens defining tumor malignancy: basis for development of anti-cancer vaccines. Adv Exp Med Biol. 491: 369-402
13. Aoki H, Satoh M, Mitsuzuka K, et al (2004). Inhibition of motility and invasiveness of renal cell carcinoma induced by short interfering RNA transfection of β1,4GalNAc transferase. FEBS Lett. 567: 203-208
14. Hamamura K, Furukawa K, Hayashi T, et al (2005). Ganglioside GD3 promotes cell growth and invasion through p130Cas and paxillin in malignant melanoma cells. Proc Natl Acad Sci USA. 102: 11041-11046
15. Ueno S, Saito S, Wada T, et al (2006). Plasma membrane-associated sialidase is up-regulated in renal cell carcinoma and promotes interleukin-6-induced apoptosis suppression and cell motility. J Biol Chem. 281: 7756-7764
16. Miyata M, Kambe M, Tajima O, et al (2011). Membrane sialidase NEU3 is highly expressed in human melanoma cells promoting cell growth with minimal changes in the composition of gangliosides. Cancer Sci. 102: 2139-2149
17. Bonardi D, Papini N, Pasini M, et al (2014). Sialidase NEU3 dynamically associates to different membrane domains specifically modifying their ganglioside pattern and triggering Akt phosphorylation. PLoS ONE. 9: e99405
18. Miyagi T, Wada T, Yamaguchi K, et al (2008). Plasma membrane-associated sialidase as a crucial regulator of transmembrane signalling. J Biochem. 144: 279-285
19. Yamaguchi H (2014). Homology modeling and structural analysis of human N-acetyl-alpha-neuraminidase 3 (NEU3). Int J Comput Bioinfo In Silico Model. 3: 473-478
20. D'Avila F, Tringali C, Papini N, et al (2013). Identification of lysosomal sialidase NEU1 and plasma membrane sialidase NEU3 in human erythrocytes. J Cell Biochem. 114: 204-211
21. Chavas LM, Tringali C, Fusi P, et al (2005). Crystal structure of the human cytosolic sialidase Neu2. Evidence for the dynamic nature of substrate recognition. J Biol Chem. 280: 469-475
22. Levitt M (1992). Accurate modeling of protein conformation by automatic segment matching. J Mol Biol. 226: 507-533
23. Fechteler T, Dengler U and Schomberg D (1995). Prediction of protein three-dimensional structures in insertion and deletion regions: a procedure for searching data bases of representative protein fragments using geometric scoring criteria. J Mol Biol. 253: 114-131
24. Bowie JU, Lüthy R and Eisenberg D (1991). A method to identify protein sequences that fold into a known three-dimensional structure. Science. 253: 164-170
25. Lüthy R, Bowie JU and Eisenberg D (1992). Assessment of protein models with three-dimensional profiles. Nature. 356: 83-85
26. Zhang C, Vasmatizis G, Cornette JL, et al (1997). Determination of atomic desolvation energies from the structures of crystallized proteins. J Mol Biol. 267: 707-726
27. Carvajal CA, Gonzalez AA, Romero DG, et al (2003). Two homozygous mutations in the 11 beta-hydroxysteroid dehydrogenase type 2 gene in a case of apparent mineralocorticoid excess. J Clin Endocr Metab. 88: 2501-2507
28. Yamaguchi H, Kamiie K, Kidachi Y, et al (2014). Structural basis for the interaction of 6-(methylsulfinyl) hexyl isothiocyanate with inducible nitric oxide synthase. Int J Comput Bioinfo In Silico Model. 3: 426-432
29. Liang J, Edelsbrunner H, Fu P, et al (1998). Analytical shape computation of macromolecules: I. Molecular area and volume through alpha shape. Proteins. 33: 1-17
30. Liang J, Edelsbrunner H, Fu P, et al (1998). Analytical shape computation of macromolecules: II. Inaccessible cavities in proteins. Proteins. 33: 18-29
31. Goto J, Kataoka R and Hirayama N (2004). Ph4Dock: pharmacophore-based protein-ligand docking. J Med Chem. 47: 6804-6811
32. Halgren TA (1996). Merck molecular force field. I. basis, form, scope, parameterization and performance of MMFF94. J Comput Chem. 17: 490-519
33. Awale M, Kumar V, Saravanan P, et al (2010). Homology modeling and atomic level binding study of Leishmania MAPK with inhibitors. J Mol Model. 16: 475-488.

*****